Characterization of ceramic hydrogen separation membranes with varying nickel concentrations

R.V. Siriwardane [a,*], J.A. Poston Jr. [a], E.P. Fisher [a], T.H. Lee [b], S.E. Dorris [b], U. Balachandran [b]

[a] *U.S. Department of Energy, National Energy Technology Laboratory, 3610 Collins Ferry Road, Morgantown, WV 26507-0880, USA*
[b] *Energy Technology Division, Argonne National Laboratory, Argonne, IL 60439, USA*

Abstract

Ceramic hydrogen separation membranes in the stoichiometric form $BaCe_{0.8}Y_{0.2}O_3$, doped with various concentrations of nickel, were characterized by utilizing X-ray photoelectron spectroscopy (XPS), scanning electron microscopy (SEM), energy dispersive spectroscopy (EDS), and atomic-force microscopy (AFM). Characterization was performed at room temperature, 550°C and 650°C, and after exposure to hydrogen. Migration of nickel to the surface and changes in both elemental composition and oxidation states were observed at elevated temperatures. The concentration of nickel significantly affects surface morphology and roughness. © 2000 Published by Elsevier Science B.V.

PACS: 82.65.F; 79.60; 61.16.C; 61.16.B
Keywords: High temperature membranes; Hydrogen separation membranes; Ceramic membranes; Surface characterization of membranes

1. Introduction

The gas stream produced during coal gasification is a significant source of hydrogen that can be utilized either in generation of clean power or as a primary chemical feed stock. Potentially, high-temperature inorganic membranes can be used to separate hydrogen from coal gasification gas streams.

Thin, dense ceramic membranes fabricated from mixed electronic and protonic conductors may provide a simple, efficient means to separate hydrogen from gas streams. Researchers at Argonne National Laboratory (ANL) [1] are developing dense, mixed-conducting ceramic membranes to separate hydrogen from various gas streams at 550–850°C (823–1123 K). These ceramic membranes are composed of barium oxide, cerium oxide and yttrium oxide in the stoichiometric form $BaCe_{0.8}Y_{0.2}O_3$. Metallic nickel was added to the oxide ceramics to promote nongalvanic hydrogen permeation. High hydrogen permeability and thermal stability are critical factors that determine the successful performance of these membranes. The initial reaction involved in this separa-

tion process is the adsorption of hydrogen at the membrane surface, where it dissociates, and the ionized hydrogen then passes through the membrane. The membrane surface plays a critical role in determining the initial reaction, and it is extremely important that we understand the surface properties if we are to successfully develop the membrane program.

The objective of this research is to characterize the surface properties of $BaCe_{0.8}Y_{0.2}O_3$ membranes with various nickel concentrations at both room and elevated temperatures. High-temperature X-ray photoelectron spectroscopy (XPS), high-temperature scanning electron microscopy (SEM)/energy dispersive spectroscopy (EDS) and atomic-force microscopy (AFM) were utilized in this study.

2. Experimental

The procedure for preparing the $BaCe_{0.8}Y_{0.2}O_3$ membranes with 30, 35, and 40 vol.% nickel has been reported previously [1].

XPS spectra were recorded with a Physical Electronics model 548 X-ray Photoelectron Spectrometer equipped with a cylindrical mirror analyzer and a 15-kV X-ray source (Physical Electronics). The system was routinely operated within a pressure range of 10^{-9}–10^{-8} Torr (1.3×10^{-7} to 1.3×10^{-6} Pa). The instrument was calibrated by using the photoemission lines E_B (copper $2p_{3/2}$) = 932.4 eV and E_B (gold $4f_{7/2}$) = 83.8 eV [2]. The binding energies were referenced to the C(1s) level at 284.6 eV for adventitious carbon. All reported intensities are experimentally determined peak areas divided by the instrumental sensitivity factors. The spectrometer sample holder is resistively heated and capable of withstanding temperatures up to 700°C. The XPS system is equipped with a sample preparation chamber that is separated from the main chamber by a gate valve. A high-precision leak valve on the sample preparation chamber permits exposure of the sample to various gases at elevated temperatures [3]. X-ray photoelectron spectroscopic analysis was also performed on the membrane samples at room temperature, i.e., 21°C (294 K), at 500°C (773 K), 650°C (923 K), and after exposure to hydrogen at 6×10^{-5} Torr for 1 h at 650°C.

X-ray microanalysis was carried out with a JEOL Model 840-A scanning electron microscope (JEOL-840A), which was routinely operated within a pressure range of 10^{-7}–10^{-6} Torr (1.3×10^{-5} to 1.3×10^{-4} Pa). The JEOL-840 A, which is equipped with a high-sensitivity, solid-state, annular backscatter electron detector, an ET-type secondary-electron detector, and a Noran Instruments Micro-Z series energy dispersive spectrometer, was interfaced to a Noran Instruments X-ray microanalysis system and a TN-5600 PAC system. Sample temperatures were obtained by using a Fullam heating substage with a VWR-1165 refrigerated constant-temperature circulator connected to the heated substage cooling jacket [4]. In this series of experiments, the depths of the X-ray interaction volumes, as computed by the Kanaya–Okayana equation, were 0.53, 0.51, and 0.54 μm for the 30, 35, and 40 vol.% nickel membranes, respectively [5].

AFM was conducted with a Quesant Instrument Model-Resolver atomic force microscope.

3. Results and discussion

3.1. Image analysis

3.1.1. Atomic-force microscopy

AFM was used to determine surface morphology and surface roughness. The AFM images in the 40-μ scan range, of membranes with 30, 35, and 40 vol.% nickel, are shown in Fig. 1; AFM images in the 10-μ range are shown in Fig. 2. Membrane surfaces do not appear smooth; nodular-type structures are apparent on all surfaces. The size of the nodules decreases with decreasing nickel concentrations and the nodules appear closer together at lower nickel concentrations. Thus, the amount of nickel influences surface morphology. Surface roughness, measured as surface height, was also affected by the amount of nickel in the membrane. Surface heights for membranes with 30, 35, and 40 vol.% nickel were 0.645, 1.04, and 1.34 μ, respectively. Surface height decreased with decreasing nickel concentration. Initial hydrogen uptake takes place at the surface of these membranes. The increase in surface roughness, as observed with

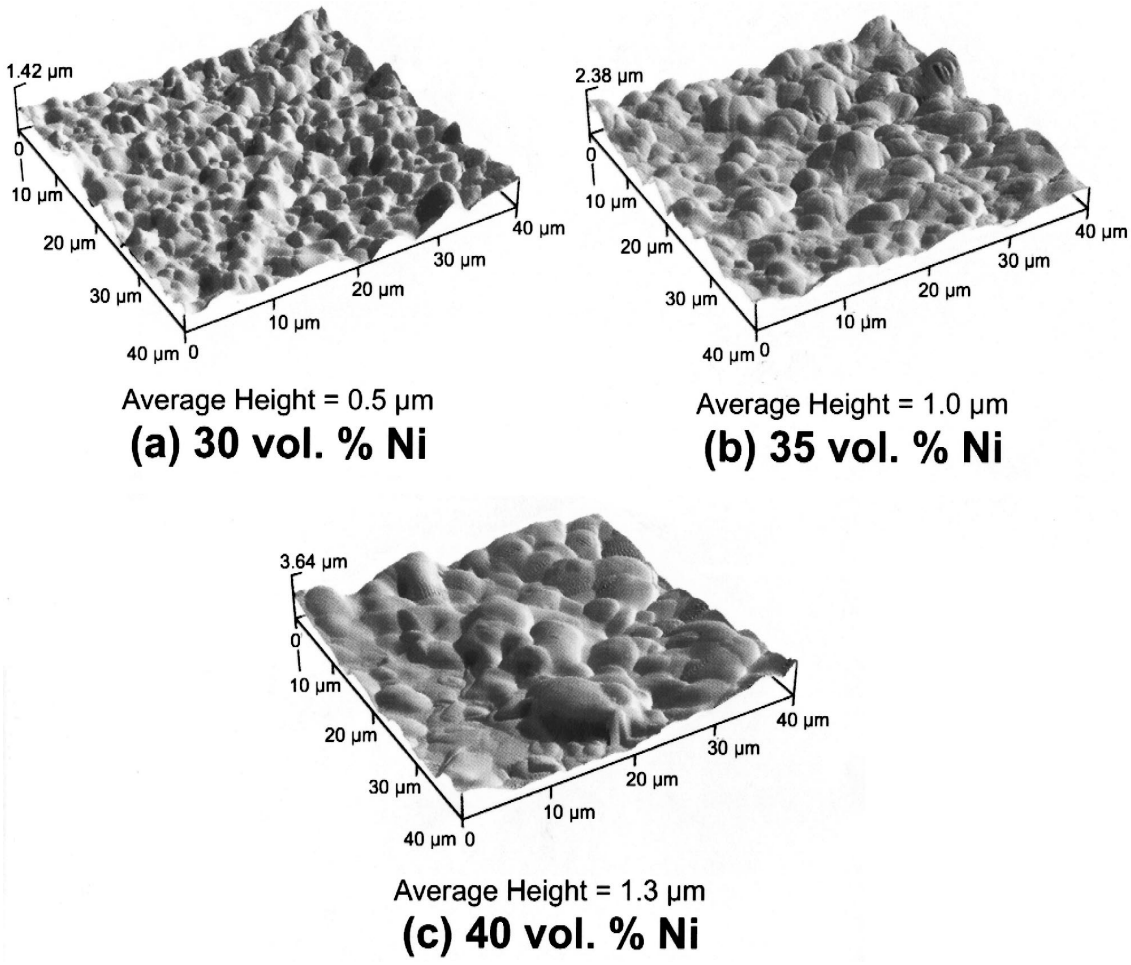

Fig. 1. AFM images of membranes with various Ni concentrations: 40 micron scans.

the increasing nickel concentration, may contribute to the increase in initial hydrogen uptake at the surface.

3.1.2. Secondary electron imaging (SEI)

SEI was used to ascertain if morphological changes occurred in the samples when heated to 575°C and after exposure to hydrogen gas (2×10^{-4} Torr for 1 h) at 575°C. Imaging of the membranes indicates that membrane surfaces exhibit a nodular-type structure similar to that observed with AFM. The appearance of the surface is "fused" and nodules appear to be larger in membranes with higher nickel concentrations, as shown in Fig. 3. The images obtained by SEI are consistent with the images obtained by AFM (Figs. 1 and 2).

No apparent morphological changes were observed when the membrane with 30 vol.% nickel was heated to 575°C and exposed to hydrogen gas at 575°C, as shown in Fig. 4. Similar observations were noted with membranes that contain 35 and 40 vol.% nickel.

3.2. X-ray photoelectron spectroscopy

XPS was used to determine the elemental composition of and oxidation states at the membrane surface, at a depth of 50 Å. Membrane samples were

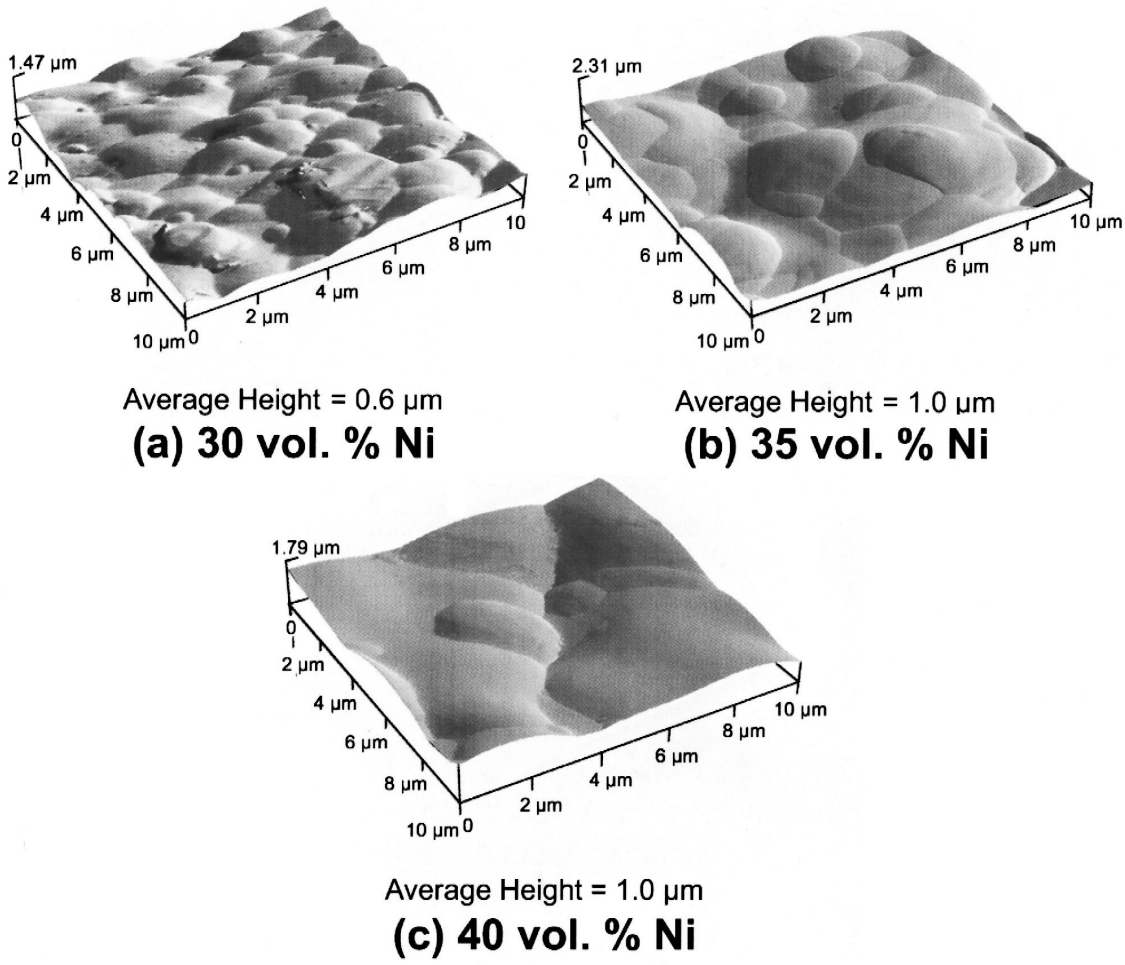

Fig. 2. AFM images of membranes with various Ni concentrations: 10 micron scans.

analyzed at room temperature, 500°C and 650°C, and after hydrogen exposures at 650°C. XPS analysis was also performed after samples were cooled to room temperature and reheated to 650°C.

3.2.1. XPS data on nickel

Nickel 2p spectra for membranes with 40 vol.% nickel at room temperature and 650°C are shown in Fig. 5. At room temperature, a weak nickel $2p_{3/2}$ peak was centered at 855.5 eV, with a satellite peak visible on the higher binding energy side of the main peak. This finding indicates that nickel at the surface of the membrane is oxidized at room temperature. When the sample was heated to 650°C, the intensity of the nickel peak increased substantially, as shown in Fig. 5, indicating that the nickel concentration at the surface increases at 650°C and migration of nickel to the surface is favored at high temperatures. A similar observation of nickel migration to the surface was observed with the other two membranes. The nickel peak at 650°C was very narrow and centered at the binding energy of 852.5 eV, which corresponds to metallic nickel [6].

The plot of the ratio of the nickel peak to the peaks of barium, cerium, and yttrium under differing experimental conditions for the membrane with 30 vol.% nickel is shown in Fig. 6. Nickel concentration, relative to the other elements is higher at 500°C

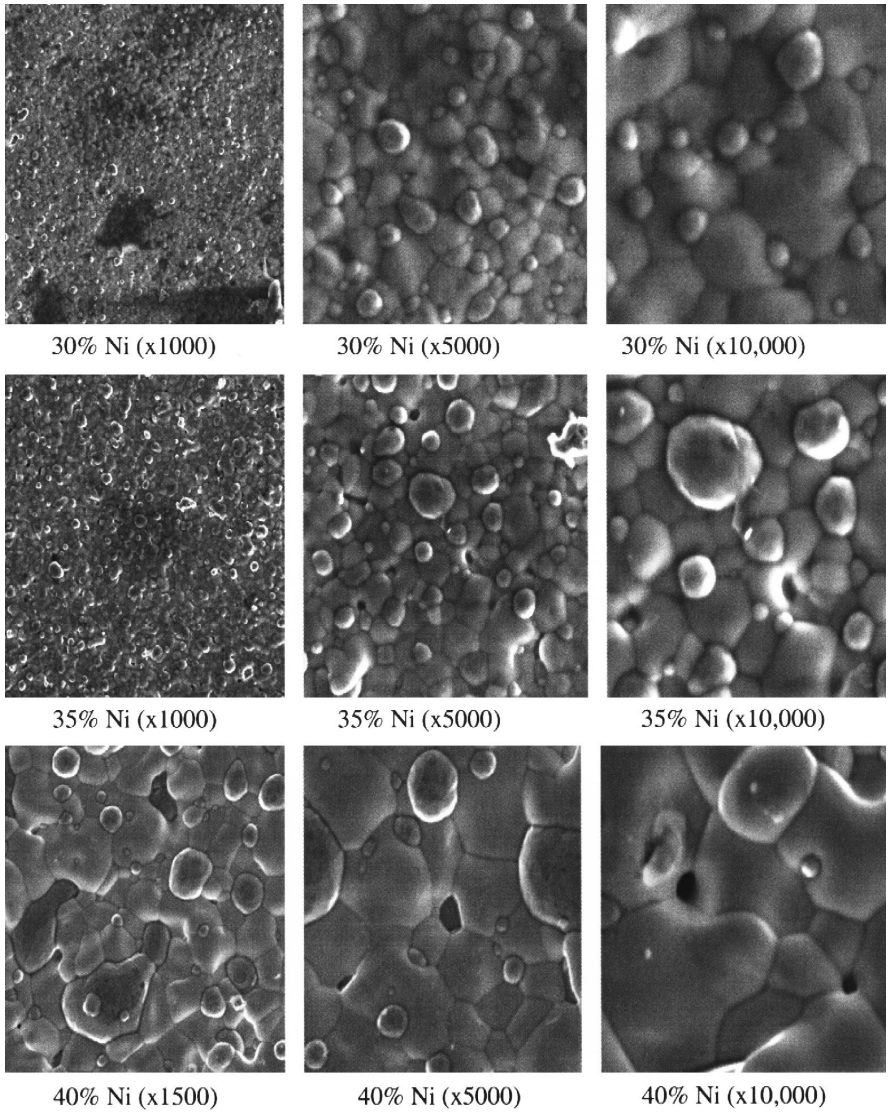

Fig. 3. Photomicrographs at various magnifications from fresh hydrogen separation membranes that contained 30, 35 and 40 vol.% Ni.

and 650°C, and after hydrogen exposures at 650°C than at room temperature. When the membrane sample was cooled to room temperature, the relative nickel concentration decreased. When the membrane was reheated to 650°C, the relative nickel concentration increased again. Clearly, nickel preferentially resides on the surface at high temperatures. The most substantial change in nickel concentration was observed with respect to barium, while the least was observed with respect to cerium.

The relative nickel concentrations under differing experimental conditions for the membrane with 35 vol.% nickel are shown in Fig. 7. The relative nickel concentration was higher at higher temperatures, which is similar to the observation when the membrane contained 30 vol.% nickel (Fig. 6). However, for the membrane with 35 vol.% nickel, the largest change in relative nickel concentration was observed with respect to cerium, whereas the smallest was observed with respect to barium. The results ob-

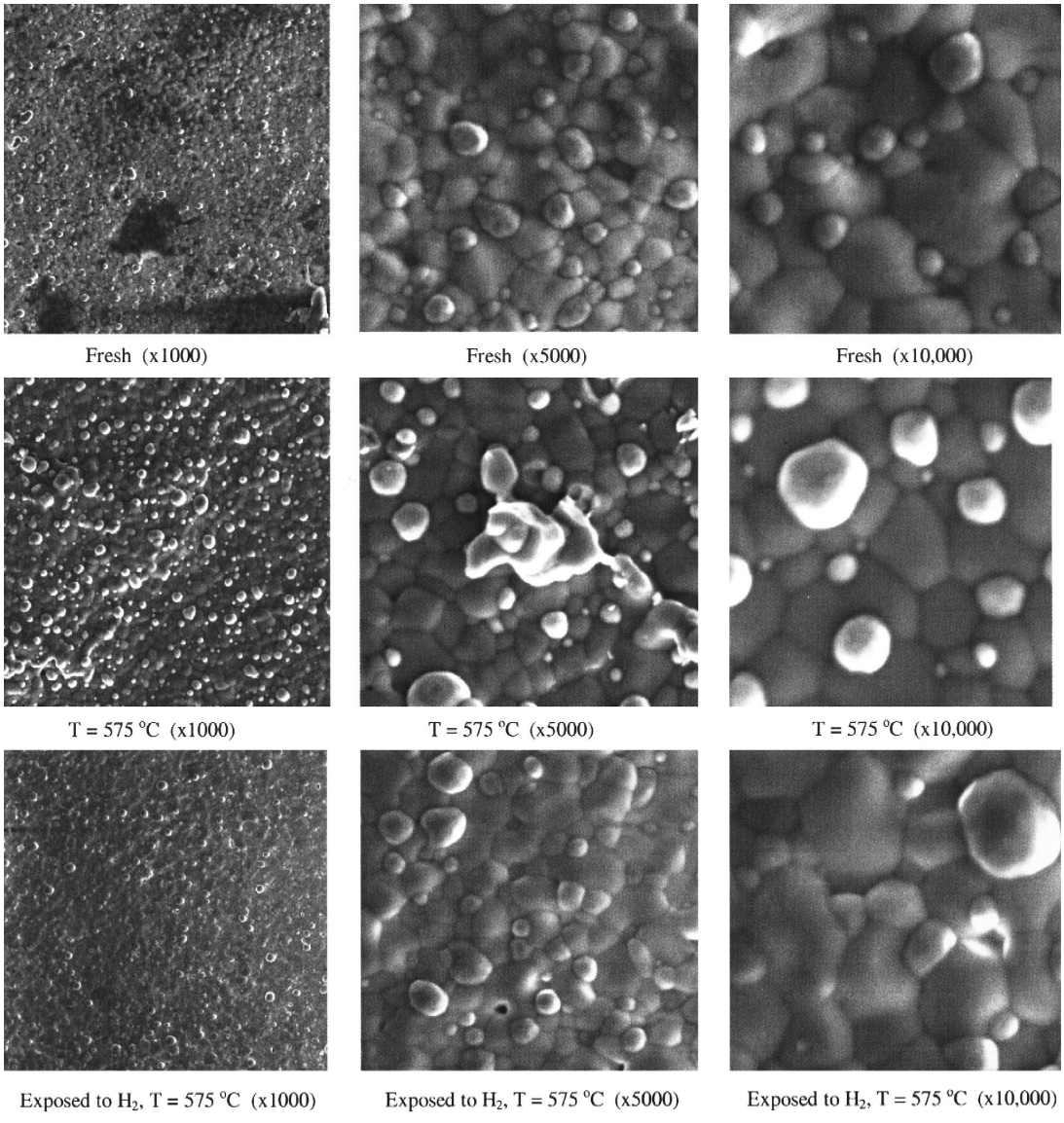

Fig. 4. Photomicrographs at various magnifications of hydrogen separation membrane that contained 30 vol.% Ni under differing conditions.

tained from the membrane with 40 vol.% nickel were similar to those obtained from the membrane with 35 vol.% nickel (Fig. 8).

$BaCe_{0.8}Y_{0.2}O_3$ exhibits protonic conductivity that is significantly higher than its electronic conductivity. To be suitable for hydrogen separation in a nongalvanic mode, i.e., without electrodes or electric power, the ceramic membranes must exhibit adequate protonic and electronic conductivities. The incorporation of nickel enhances the electronic conductivity of the membrane. Hydrogen, initially adsorbed at the surface, dissociates at the surface to form hydrogen atoms before becoming ionized. The presence of nickel at the surface may enhance this initial surface reaction.

The rate of nongalvanic hydrogen permeation N through a mixed-conducting membrane is described [1] by:

$$N = \sigma_{amb}(E_N - \eta)/2FL, \quad (1)$$

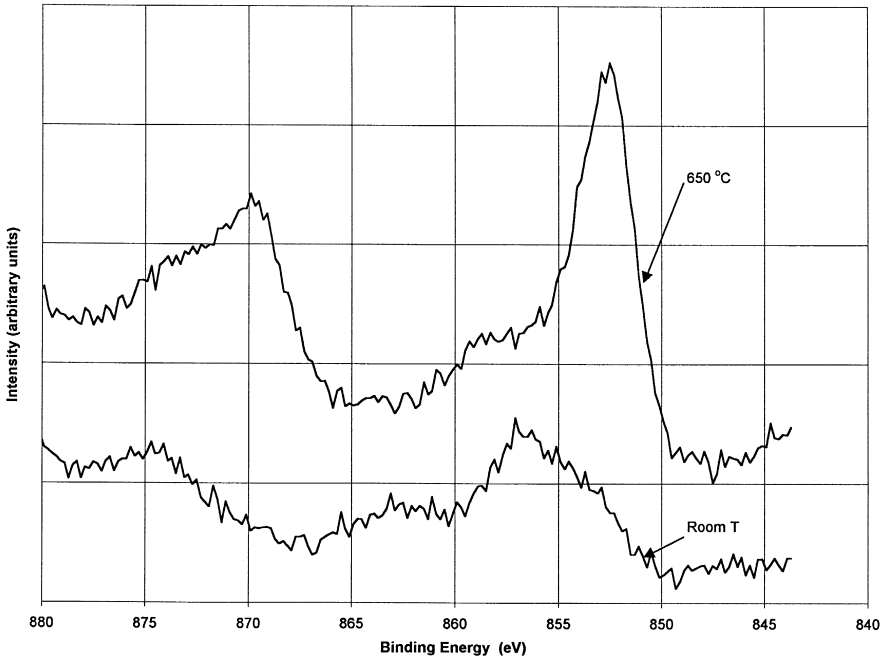

Fig. 5. Ni 2p spectra of membrane with 40 vol.% Ni at room temperature and 650°C.

where L is the thickness of the membrane, F is the Faraday constant, η is the interfacial overpotential, E_{N} is the Nernst potential across the membrane, and σ_{amb} is the ambipolar conductivity of the membrane.

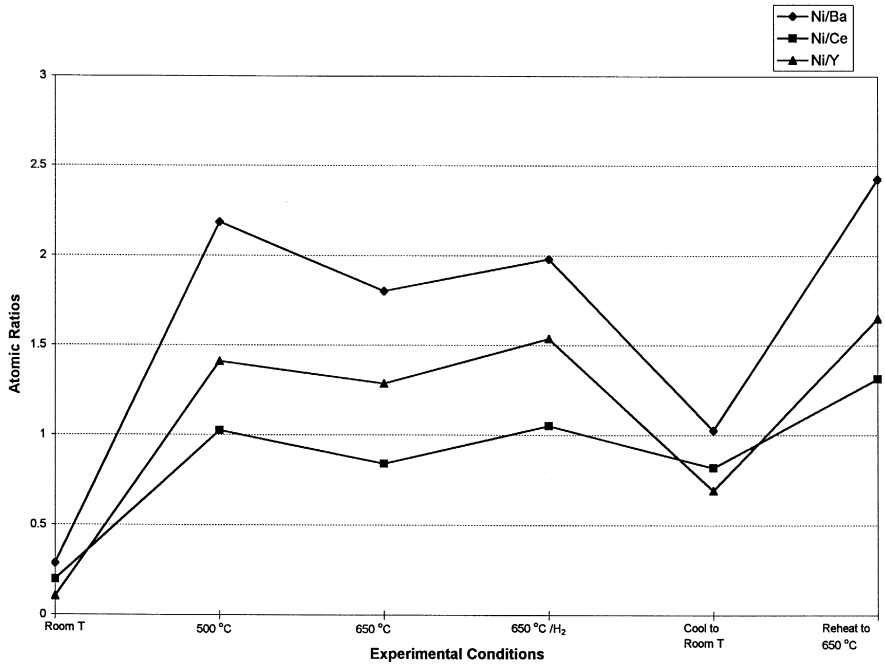

Fig. 6. Atomic ratios of Ni to Ba, Ce and Y as a function of experimental conditions for membrane with 30 vol.% Ni.

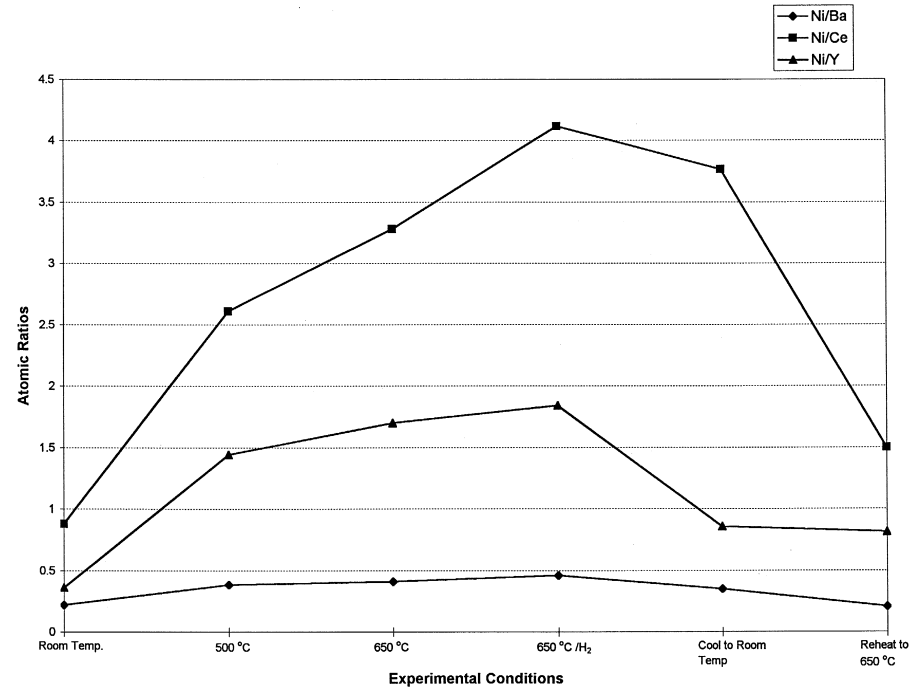

Fig. 7. Atomic ratios of Ni to Ba, Ce and Y as a function of experimental conditions for membrane with 35 vol.% Ni.

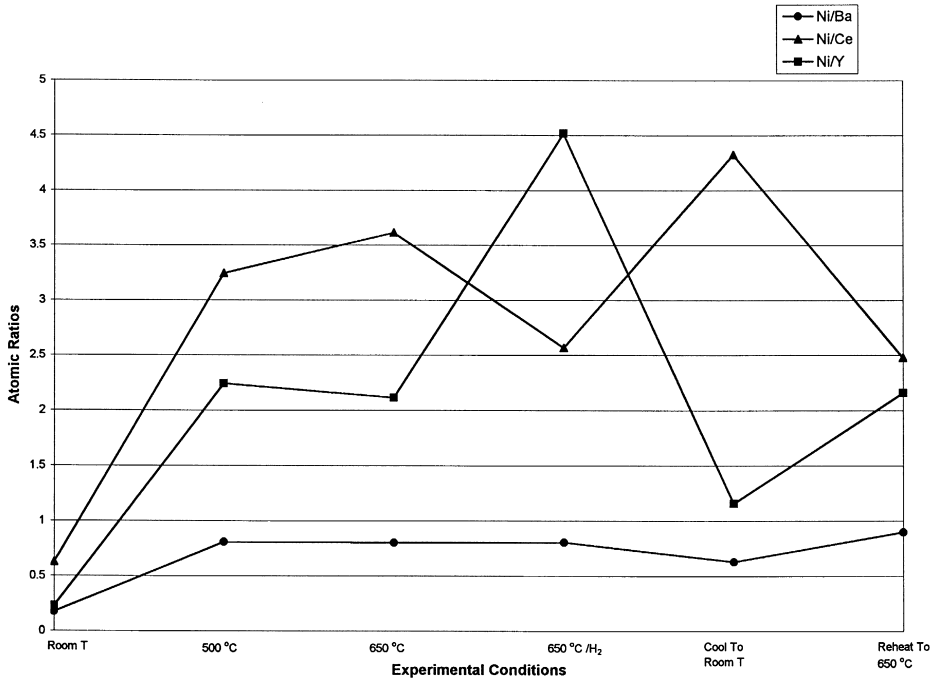

Fig. 8. Atomic ratios of Ni to Ba, Ce and Y as a function of experimental conditions for membrane with 40 vol.% Ni.

Both electronic and protonic conductivity contribute to the ambipolar conductivity. An increase in the ambipolar conductivity contributes to the increase in permeation of hydrogen (N) through the membrane.

Eq. (1) can be rewritten as:

$$E_N/2FN = \eta/2FN + L/\sigma_{amb}, \quad (2)$$

and plotting the left-hand side of the equation against sample thickness yields the interfacial polarization R_p and the ambipolar conductivity σ_{amb}, as defined by:

$$R_p = (E_N/2FN)_{L\to 0}. \quad (3)$$

Incorporation of a metal phase enhances the hydrogen permeation of the membrane in several ways. It increases the ambipolar conductivity by increasing its electronic conductivity and it decreases the interfacial polarization resistance, both of which increase the permeation rate, as shown in Eq. (1).

The migration of nickel to the surface at high temperatures will decrease the interfacial polarization resistance (R_p) and this, in turn, will contribute to the increase in hydrogen permeation (N) of the membrane. However, if all of the nickel migrates to the surface, eventually, depletion of the nickel in the bulk may occur. Such a depletion will decrease the ambipolar conductivity, and thereby contribute to the decrease in the permeation rate, as in Eq. (1).

It was reported [1] that interfacial resistance dominates in the $BaCe_{0.8}Y_{0.2}O_3$ membranes at lower temperatures and nickel migration to the surface at higher temperatures might contribute somewhat to lowering the interfacial resistance at high temperatures.

The conductivity measured in the presence of 4% hydrogen of the membranes with 30% and 40% nickel were 0.03 and 200 Ω^{-1} cm^{-1}, respectively. Since the conductivity is highest for the membrane with the 40% nickel the permeation rate (0.1 $cc/min/cm^2$) is expected to be highest for the membrane with 40% nickel. The AFM images showed the highest surface height for the membrane with 40% nickel. Migration of nickel to the surface observed at high temperature was also highest for the membrane with 40% nickel.

3.2.2. XPS data on cerium

The cerium 3d spectra of the membrane with 30 vol.% nickel at room temperature and 650°C are shown in Fig. 9. The $3d_{5/2}$ and $3d_{3/2}$ peaks were at 882.4 and 899.7 eV, respectively. Intense satellite peaks (at 886.1 and 905 eV) appeared on the higher

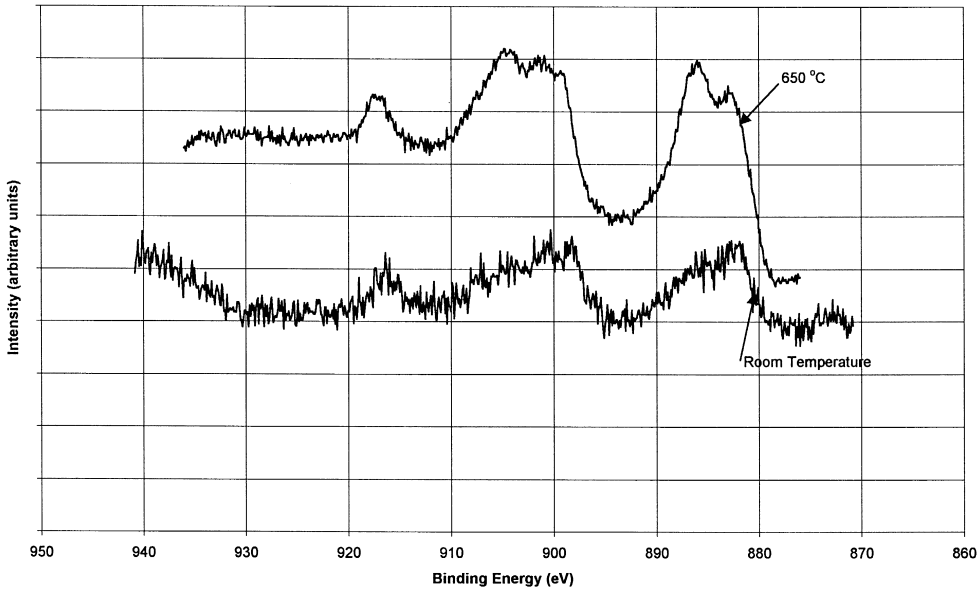

Fig. 9. Ce 3d spectra for membrane with 30 vol.% Ni at room temperature and 650°C.

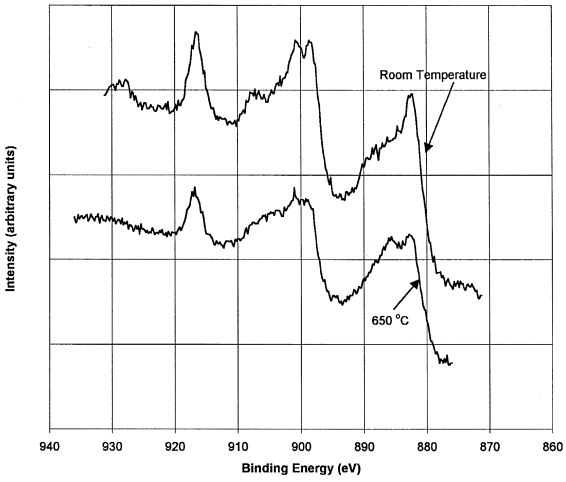

Fig. 10. Ce 3d spectra of Ce(IV) oxide at room temperature and 650°C.

binding energy side of the main peaks. A third satellite peak at the 916.4 eV was also visible. The cerium 3d spectrum of Ce(IV) oxide is shown in Fig. 10. The cerium 3d spectrum of the membrane with 30 vol.% nickel at room temperature was very similar to that of the Ce(IV) oxide standard, indicating that the cerium in the membrane is in the Ce^{+4} state [7–10]. When the membrane was heated to 650°C, the structure of the $3d_{5/2}$ and $3d_{3/2}$ peaks changed (Fig. 10). The main peaks appeared at 882.8 and 886.1 eV, with strong secondary peaks at a higher binding energy of the main peaks (886.1 and 904.8 eV), indicating the formation of Ce^{+3} at 650°C [10]. The satellite peak at 916 eV was present, but the intensity of this peak relative to the intensities of the major $3d_{5/2}$ and $3d_{3/2}$ peaks of the heated sample is lower than the intensity observed at room temperature. This again indicates that the membrane with 30 vol.% nickel consists of cerium in the $+3$ and $+4$ states at 650°C. The cerium spectrum after exposure to hydrogen at 650°C was very similar to the spectrum before exposure to hydrogen at this temperature.

The changes in the cerium 3d spectrum for the membrane with 35 vol.% nickel were very similar to that of membrane with 40 vol.% nickel, but differed from the changes noted for the membrane with 30 vol.% nickel. The cerium 3d spectra of the membrane with 35 vol.% nickel at room temperature and at 650°C are shown in Fig. 11. The satellite peak at

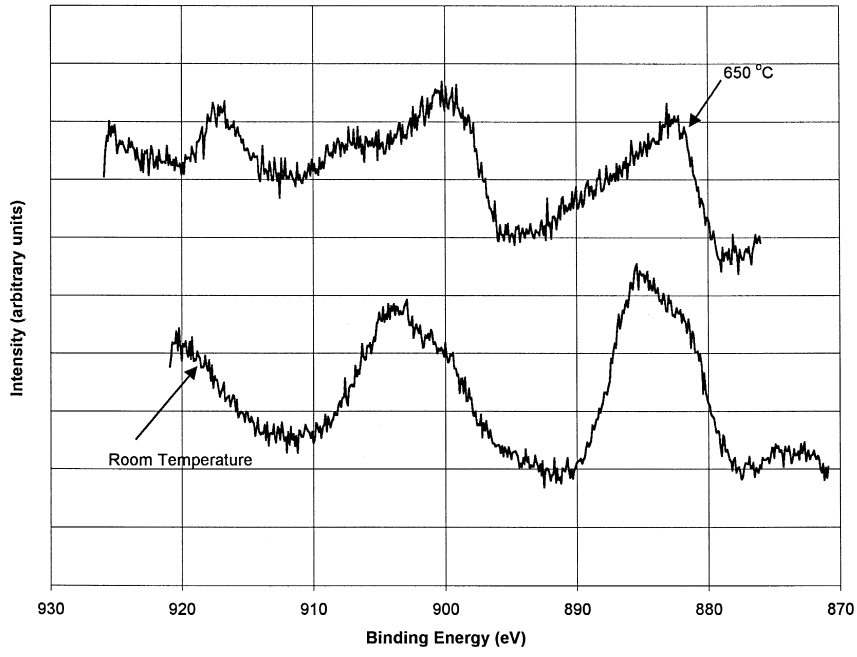

Fig. 11. Ce 3d spectra of membrane with 35 vol.% Ni at room temperature and 650°C.

916.6 eV was not present in these samples, indicating that cerium is in the +3 state at room temperature [10]. At 650°C, the structure of the cerium $3d_{5/2}$ peaks changed, with the satellite peaks appearing on the higher binding energy side of the main peak (Fig. 11). The satellite peak at 916.6 eV also appeared at 650°C, indicating the presence of Ce^{+4} in the sample. Thus, the cerium in membranes that contained 35 and 40 vol.% nickel exists in the +3 state at room temperature, but changes to Ce^{+4} at 650°C. Oxidation of Ce^{+3} to Ce^{+4} may be due to an interaction between cerium and other oxides in the sample.

Membranes of $BaCe_{0.8}Y_{0.2}O_3$ are prepared by adding the dopant material, yttrium, to the $BaCeO_3$. In $BaCeO_3$, cerium is in the +4 state and, during the preparation of $BaCe_{0.8}Y_{0.2}O_3$, a portion of the Ce^{+4} is replaced by yttrium in the +3 state. Because the dopant is in the lower oxidation state (less positive charge when compared with the original Ce^{+4}), these charges are initially compensated for by oxygen vacancies (V_0'') [11], as shown in the reaction:

$$Y^{+3} \rightarrow Y_{Ce}^{\cdot} + V_0''.$$

The oxygen vacancies may be in equilibrium with electron holes:

$$V_0'' + O_2 \rightarrow O_0^x + 2h^{\cdot},$$

where O_0^x and $h^{\cdot}$ are oxide ions in a normal lattice site and hole, respectively.

In the presence of hydrogen, the following reaction can occur and lead to proton conduction:

$$H_2 + 2h^{\cdot} \rightarrow 2H^{\cdot}.$$

Analysis of the membranes by XPS indicates that cerium is present in the +3 as well as in the +4 state. The presence of Ce^{+3} may contribute to the formation of additional oxygen vacancies, which may contribute to proton conduction. The reason for the formation of Ce^{+3} in these membranes is not clear but it could be due to interaction between metallic nickel and Ce^{+4}. However, if the concentration of Ce^{+3} increases too much, the interaction among the Ce^{+3} entities may reduce their mobility and decrease the conductivity.

The ratio of cerium to other metals in the membrane with 30 vol.% nickel are shown in Fig. 12. When the sample was heated to 650°C, there was a slight increase in the cerium concentration with respect to barium and yttrium, but there was a decrease with respect to nickel. The relative proportions of cerium in the membranes with 35 vol.% nickel are shown in Fig. 13. Only the Ce/Y ratio increased when the sample was heated to 650°C. Similar observations were noted for the membrane with 40 vol.% nickel. However, this observation differs from the observation that was noted for the membrane with 30 vol.% nickel, where both Ce/Y and Ce/Ba increased when the sample was heated.

3.2.3. XPS data on yttrium

The yttrium 3d spectra of the membrane with 40 vol.% nickel at room temperature and at 650°C are shown in Fig. 14. At room temperature, the yttrium peak appears to be a single peak at a binding energy of 158.4 eV. However, at 650°C, a secondary peak appears on the higher binding energy side (161.8 eV) of the main peak at 157.9 eV (Fig. 14). The lower binding energy of the main peak indicates that yttrium changes to a less electro-positive state at 650°C. The secondary peak remained after exposure to hydrogen and after cooling the sample to room temperature. Similar observations were noted for the membrane with 35 vol.% nickel, but the intensity of the secondary peak at 650°C was lower when compared with the membrane with 40 vol.% nickel. These results differ from those obtained for the membrane with 30 vol.% nickel, where the binding energy of yttrium was 156.6 eV at room temperature and 157.9 eV at 650°C. The secondary peak was not clearly visible at 650°C. The increase in binding energy for the main peak indicates that yttrium became more electro-positive at 650°C for the membrane with 30 vol.% nickel. The 3d spectra of pure yttrium oxide (Y_2O_3) at room temperature and 650°C are shown in Fig. 15. A secondary peak was not observed when the sample was heated to 650°C, indicating that the changes observed at 650°C in the yttrium 3d spectra of membranes with 35 and 40 vol.% nickel may be due to the interaction of yttrium with other elements, and possibly the presence of nickel, inasmuch as the secondary peak was most visible with membranes with higher nickel concentrations.

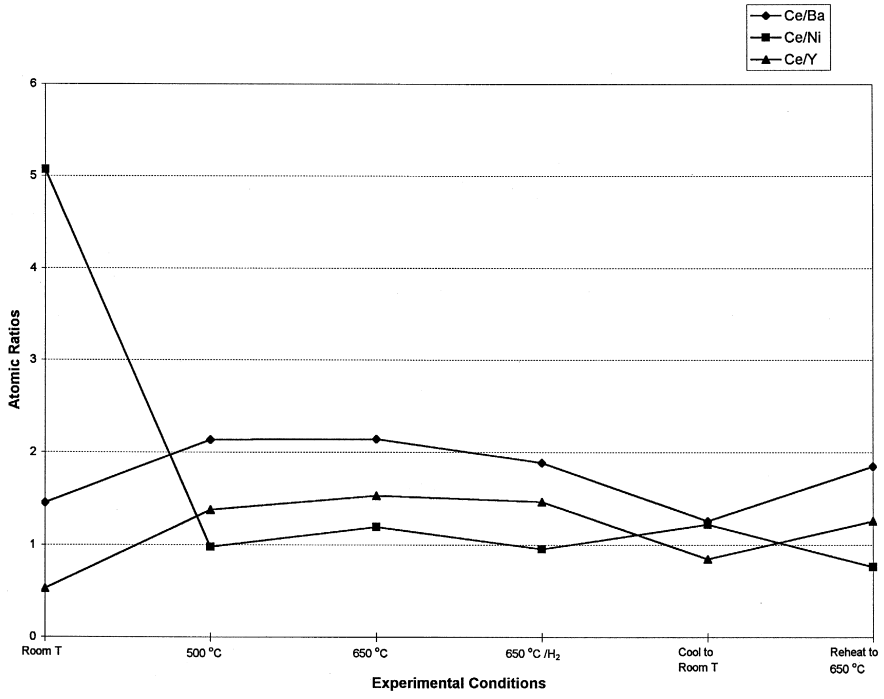

Fig. 12. Atomic ratios of Ce to Ba, Ni and Y as a function of experimental conditions for membrane with 30 vol.% Ni.

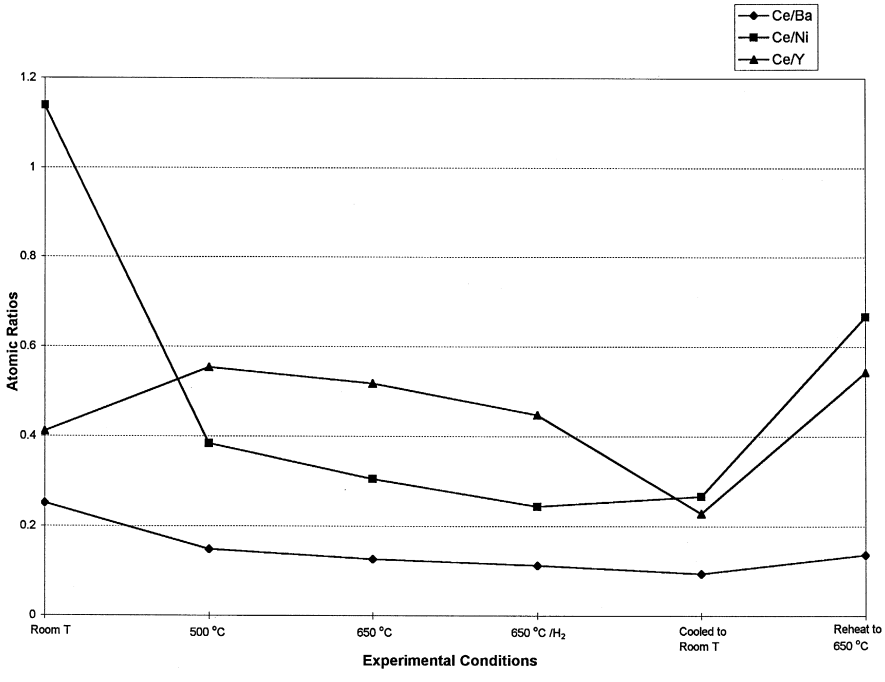

Fig. 13. Atomic ratios of Ce to Ba, Ni and Y as a function of experimental conditions for membrane with 35 vol.% Ni.

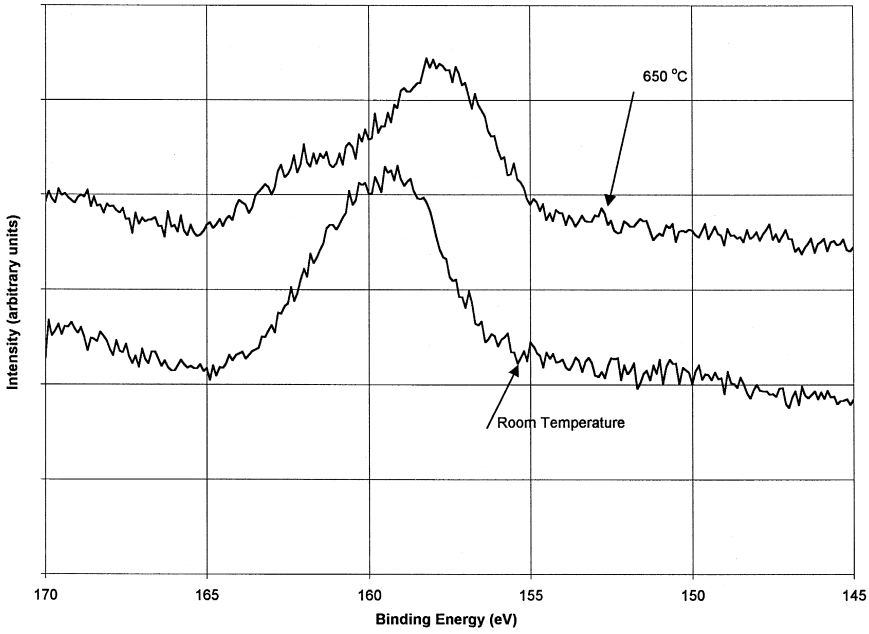

Fig. 14. Y $3d_{5/2}$ spectra of membrane with 40 vol.% Ni at room temperature and 650°C.

The analysis of the intensities of the yttrium peak relative to nickel, cerium, and barium for the membrane with 40 vol.% nickel indicated that the yttrium concentration decreases with respect to other elements when the sample was heated from room temperature to 500°C and 650°C. The most significant change was observed with respect to nickel, whereas the smallest change was observed with respect to

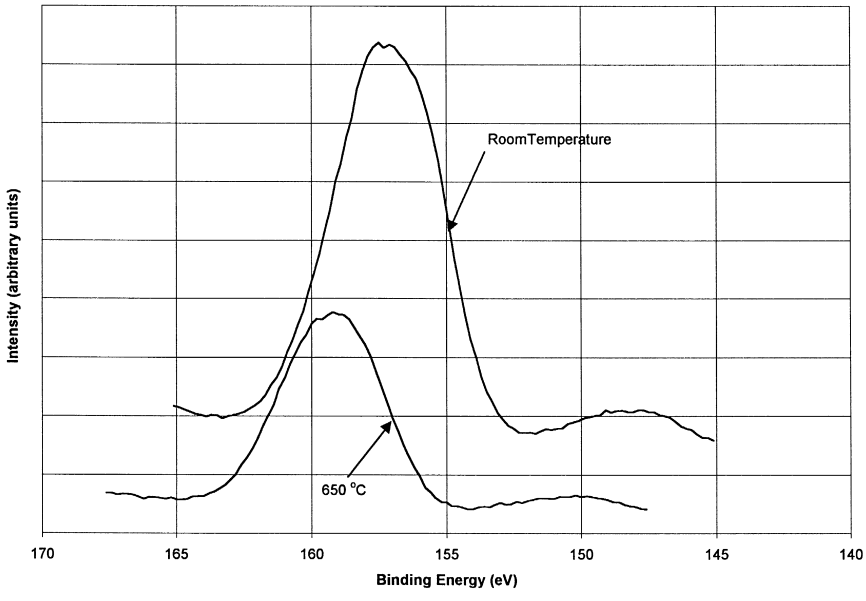

Fig. 15. Y $3d_{5/2}$ spectra of pure Y_2O_3 at room temperature and 650°C.

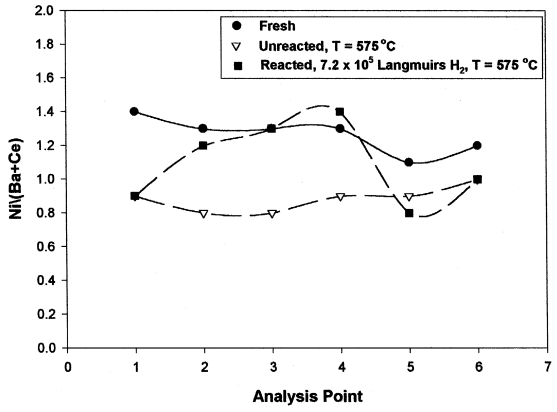

Fig. 16. Results of microanalysis of hydrogen separation membranes containing 30, 35 and 40 vol.% Ni.

barium. A similar observation was noted for the membrane with 35 vol.% nickel. A decrease in the relative yttrium concentration was also observed at higher temperatures for the membrane with 30 vol.% nickel; this observation is similar to observations noted for the other membranes, but the smallest change was observed with respect to cerium instead of barium.

3.2.4. XPS data on barium

The XPS barium $3d_{5/2}$ spectra at room temperature were very similar to those at 650°C for all three membranes. The binding energy of 780 eV indicated that barium is in the $+2$ state.

For all three membranes, the concentration of barium with respect to nickel decreased at the higher temperature. Both Ba/Ce and Ba/Y increased slightly at higher temperatures for membranes with 35 and 40 vol.% nickel. The observation noted for the membrane with 30 vol.% nickel differed; only Ba/Y increased at higher temperatures.

3.3. SEM / energy dispersive microscopy

3.3.1. X-ray microanalysis

Unreacted membrane prepared at ANL served as the microanalysis reference material. The data collected from unreacted membranes served as an indication of the material's homogeneity. The composition of the reference material was based on the stoichiometric ratios of the elements in the fresh membrane ($BaCe_{0.8}Y_{0.2}O_3$).

Single element ratios were not calculated because some of the L-series spectral peaks of barium and cerium overlapped. Therefore, the data are presented in terms of the ratio of Ni/(Ba + Ce). Standard peak subtraction/deconvolution was not effective because of compositional variations and changes that occur during heating and exposure to hydrogen. Microanalysis results of the membrane with 40 vol.% nickel at room temperature, 575°C, and after exposure to hydrogen (2×10^{-4} Torr for 1 h) at 575°C are shown in Fig. 16. The arithmetic mean and standard deviation of the data for all three membranes are listed in Table 1.

The ratio of Ni/(Ba + Ce) at 575°C was lower than that at room temperature for the membrane with 40 vol.% nickel, indicating that there is a decrease in the relative nickel concentration in the X-ray analysis volume (Fig. 16, Table 1). Analysis volume in X-ray microanalysis is closer to the bulk (0.5 μ range) than the XPS (50 Å) volume. The increase in nickel concentration at elevated temperature, observed with XPS, indicates that migration of nickel occurs from the bulk to the surface at higher temperatures. The increase in nickel at the surface should be associated with a decrease in nickel concentration in the bulk region. Such an associated decrease is consistent with observations noted with the X-ray microanalysis for the membrane with 40 vol.% nickel; a decrease was noted in the relative nickel concentration at higher temperatures. The results of the analysis after exposure to hydrogen were inconclusive.

In the membrane with 35 vol.% nickel, the change in the Ni/(Ba + Ce) ratio after heating from room temperature to 575°C was not significant as shown in Table 1. Inconsistencies in data obtained with the membrane with 30 vol.% nickel precluded the determination of compositional changes (Table 1). Lower nickel concentrations and the overlapping of barium and cerium peaks may have contributed to this observation.

Table 1
Arithmetic mean and standard deviation of Ni/(Ba + Ce) experimental data obtained from X-ray microanalysis

Membrane	Fresh	575°C	7.2×10^{-5} Langmuirs of H_2 at 575°C
40 vol.%	1.3 ± 0.09	0.9 ± 0.07	1.1 ± 0.2
35 vol.%	0.9 ± 0.07	1.1 ± 0.05	1.1 ± 0.06
30 vol.%	0.8 ± 0.05	0.8 ± 0.05	0.75 ± 0.05

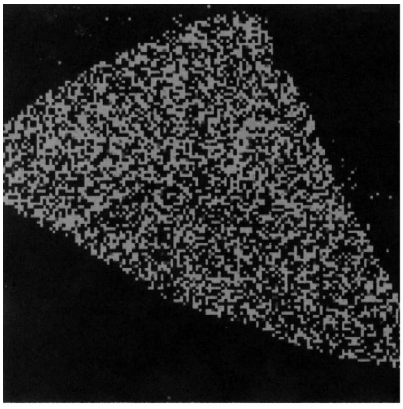

30% Ni, Fresh

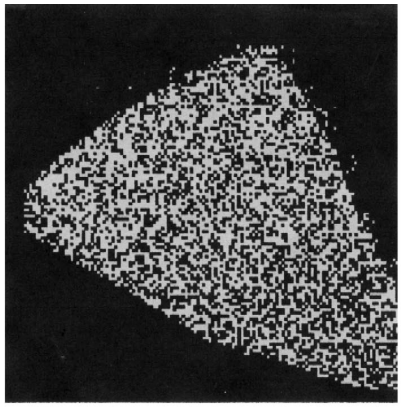

30% Ni, T = 575 °C

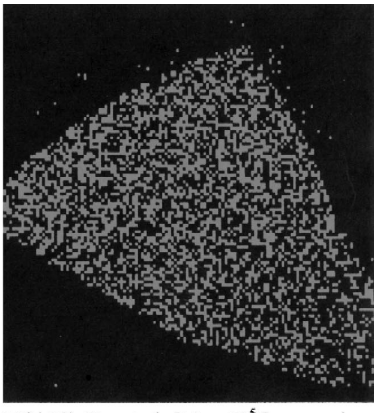

30% Ni, Reacted: 7.2 x 10^5 Langmuirs H_2, T = 575 °C

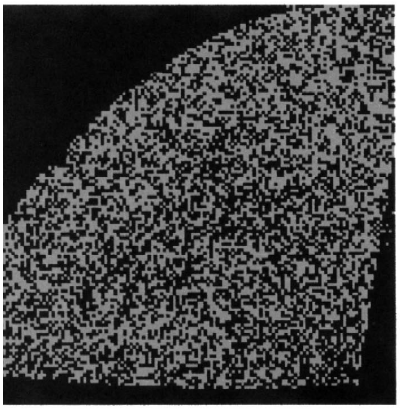

35% Ni, Fresh

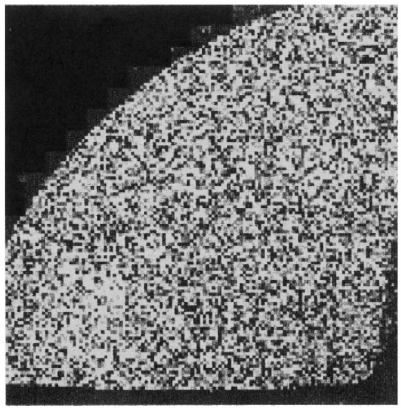

35% Ni, T = 575 °C

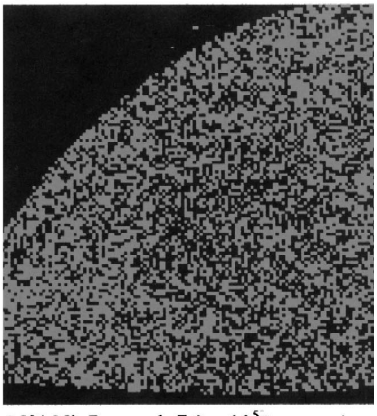

35% Ni, Reacted: 7.2 x 10^5 Langmuirs H_2, T = 575 °C

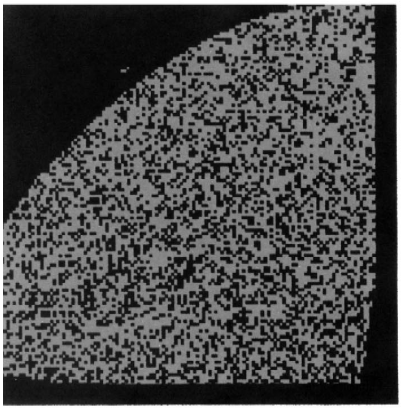

40% Ni, Fresh

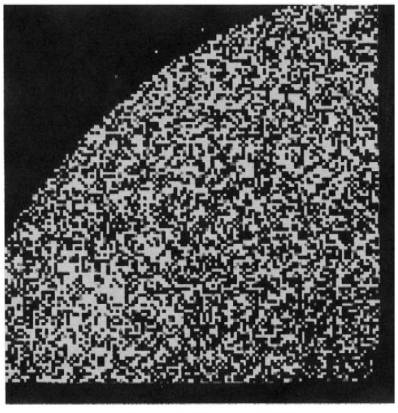

40% Ni, T = 575 °C

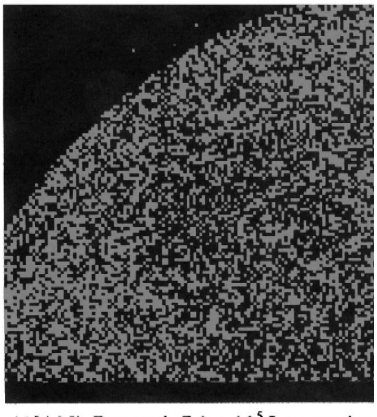

40% Ni, Reacted: 7.2 x 10^5 Langmuirs H_2, T = 575 °C

Fig. 17.

3.3.2. X-ray mapping

X-ray maps of the three membranes were obtained to determine qualitative changes in elemental distribution during heating to 575°C and after hydrogen exposures at 575°C. The elemental maps of nickel for the membranes are shown in Fig. 17. Qualitative analysis indicated that all elements were uniformly distributed at room temperature and remained uniformly distributed at 575°C, and after exposure to hydrogen at 575°C.

Nickel is incorporated in the form of nickel oxide (2–4 μm size) and nickel oxide is reduced in the presence of hydrogen at high temperature during the preparation of the membranes. Therefore, the nickel particles are expected to be fine and form a three-dimensional network to promote the electronic conductivity. Uniform distribution of nickel as fine particles (not large clusters) is essential for the formation of the three-dimensional network.

3.4. Conclusions

The nickel concentration of membranes significantly affects their surface properties. Variations in surface morphology and surface roughness were associated with nickel concentrations of the investigated membranes. Both AFM and SEM imaging analysis indicate that membrane surfaces were not smooth. Instead, a nodular-type structure was apparent on all surfaces. The size of the nodules decreased with decreasing nickel concentration and the nodules appeared closer together at lower nickel concentrations. Surface height, which is a measure of surface roughness, increased with increasing nickel concentration.

Migration of nickel, with respect to the other elements in the membrane, was observed at the surface for all of the membranes that were studied when samples were heated to higher temperatures. Upon cooling the membranes to room temperature, the concentration of nickel at the surface returned to values that were similar to those under preheating conditions. Migration of nickel to the surface may enhance hydrogen permeation by enhancing surface exchange reaction.

In the membrane that contained 30 vol.% nickel, cerium was in the + 4 state at room temperature but formation of some Ce^{+3} occurred at 650°C. In the membranes that contained 35 and 40 vol.% nickel, cerium was in the + 3 state at room temperature, and in the + 4 state at 650°C. Changes in relative cerium concentration were similar for membranes with 35 and 40 vol.% nickel but differed from the changes observed in the membrane with 30 vol.% nickel. The presence of cerium in the + 3 state may contribute to the formation of additional oxygen vacancies, which may contribute to better proton transport through the membranes.

Formation of a secondary yttrium peak was observed at 650°C for membranes that contained 35 and 40 vol.% nickel, a finding that differed from the observations noted for membranes that contained 30 vol.% nickel. The presence of nickel may have contributed to the formation of this secondary yttrium peak. The relative yttrium concentration decreased when the membranes were heated from room temperature to 650°C. Changes in the elemental distribution at the surface appear to be similar for membranes that contained 35 and 40 vol.% nickel, but differed from changes noted in the membrane with 30 vol.% nickel. The qualitative elemental distribution observed by X-ray mapping indicated a uniform distribution of elements in the membranes at room temperature and at 650°C.

Acknowledgements

The work at ANL was supported by the U.S. Department of Energy, National Energy Technology Laboratory, under contract W-31-109-Eng-38.

References

[1] U. Balachandran, T.H. Lee, S.E. Dorris, Proceedings of Sixth Annual International Pittsburgh Coal Conference, Pittsburgh, PA, Oct., 1999.
[2] C.D. Wagner, W.M. Riggs, L.E. Davis, J.F. Moulder, G.E. Muilenberg, in: G.E. Muilenberg (Ed.), Handbook of X-ray and Ultraviolet Photoelectron Spectroscopy, 1979, Perkin Elmer, Physical Electronics Division.
[3] R.V. Siriwardane, J.P. Poston, Appl. Surf. Sci. 68 (1993) 65–80.
[4] J.A. Poston, Scanning 17 (1995) 316–321.
[5] J.I. Goldstein, D.E. Newbury, P. Echlin, D.C. Joy, C. Fiori, E. Lifshin, Scanning Electron Microscopy and X-ray Microanalysis, Plenum, New York, 1984, Chap. 3.

[6] K.S. Kim, R.E. Davis, J. Electron Spectrosc. Relat. Phenom. 1251 (1973) 1972.
[7] J. Ding, L.T. Weng, S.J. Yang, Phys. Chem. 100 (1996) 11120–11121.
[8] M. Coldea, M. Neumann, St. Lutkehoff, S. Mahl, R.J. Coldea, Alloys Comp. 278 (1998) 72–79.
[9] E.S. Putna, R.J. Gorte, J.M. Vohs, G.W. Graham, J. Catal. 178 (1998) 598–603.
[10] D.A. Creaser, P.G. Harrison, M.A. Morrison, B.A. Wolfindale, Catal. Lett. 23 (1994) 247–251.
[11] H. Iwahara, in: P. Colomban (Ed.), Proton Conductors, Cambridge Univ. Press, Cambridge, 1992, p. 122.